Beam Spray Thresholds in ICF-Relevant Plasmas

David Turnbull,[1,*] Joseph Katz,[1] Denise E. Hinkel,[2] Pierre Michel,[2] Thomas Chapman,[2] Laurent Divol,[2] Eugene Kur,[2] Steve MacLaren,[2] Avram L. Milder,[1] Mordecai Rosen,[2] Alex Shvydky,[1] George B. Zimmerman,[2] and Dustin H. Froula[1]

[1]*University of Rochester Laboratory for Laser Energetics, 250 E River Road, Rochester, New York 14623, USA*

[2]*Lawrence Livermore National Laboratory, 7000 East Avenue, Livermore, California 94550, USA*

(Received 11 March 2022; accepted 15 June 2022; published 5 July 2022)

Beam spray measurements suggest thresholds that are a factor of ≈2 to 15× less than expected based on the filamentation figure of merit often quoted in the literature. In this moderate-intensity regime, the relevant mechanism is forward stimulated Brillouin scattering. Both weak ion acoustic wave damping and thermal enhancement of ion acoustic waves contribute to the low thresholds. Forward stimulated Brillouin scattering imparts a redshift to the transmitted beam. Regarding the specific possibility of beam spray occurring outside the laser entrance holes of an indirectly driven hohlraum, this shift may be the most concerning feature owing to the high sensitivity of crossed-beam energy transfer to the interacting beam wavelengths in the subsequent overlap region.

DOI: 10.1103/PhysRevLett.129.025001

Understanding the limits of controlled laser-beam propagation in plasma has long been a central question in laser-plasma research, including every branch of inertial confinement fusion. It is well known that laser-plasma instabilities (LPI) degrade beam propagation, and the operable parameter space for experiments is often tightly constrained by the need to avoid the worst impacts of LPI [1–6]. The less prominent role of LPI in modern, low-gas-fill, laser-indirect-drive (LID) hohlraums [7,8] has enabled significant increases in fusion yield [9,10]. However, it has become clear that *low* LPI does not mean *no* LPI: for example, implosion symmetry remains highly sensitive to crossed-beam energy transfer [11–15]. Identifying LPI processes that are active in LID hohlraums therefore remains a key area of research.

Recent radiation-hydrodynamic simulations of LID implosions that included external laser-entrance-hole hardware showed that ablation of an aluminum retaining ring by x rays emitted from the hohlraum interior can produce a region of plasma where the outer cones might be at risk of filamentation prior to entering the hohlraum. (For a general description of a typical LID hohlraum configuration, see, e.g., Fig. 1 of Ref. [8].) This external hardware has not traditionally been included in the vast majority of implosion simulations to date, and it has been conjectured that its neglect contributed to the longstanding inability to reliably predict hohlraum drive and implosion symmetry in simulations [16]. This hypothesis sparked renewed interest in understanding the precise onset of filamentation (beam spray) in typical plasmas, as well as the ramifications for beam propagation when thresholds are exceeded.

Early theoretical work identified the conditions under which a plane wave beam would break up into hot spots due to ponderomotive [17], thermal [18,19], or relativistic [20] effects. The introduction of phase plates effectively bypassed this step by making speckled beams the initial condition [21–23]. This did not necessarily eliminate angular spreading, however, because intense individual hot spots within the imposed speckle pattern can still self-focus and cause instability [24,25]. Simulations found that speckle self-focusing provided a strong seed for forward stimulated Brillouin scattering (FSBS), which could quickly dominate the resulting angular spreading of the beam [26–28]. Moreover, it was later shown that FSBS can induce temporal incoherence and beam spray even when all of the speckles remain below the self-focusing threshold [29–31]. A key identifying signature of FSBS is the redshift imparted to the beam, which increases with scattering angle. This mechanism is sometimes also referred to as plasma-induced incoherence [32–34]. In flowing plasmas, it can cause beam bending as well [35–37].

Various thresholds have been proposed for the onset of beam spray. The filamentation figure of merit—FFOM $= 10\langle I_{14}\rangle\lambda^2(n_e/n_c)(3/T_e)(f^{\#}/8)^2$, with average intensity in units of 10^{14} W/cm^2, laser wavelength in microns, and electron temperature in keV—remains widely used, with beam spray expected for FFOM > 1 in the case of a linearly polarized beam with no temporal smoothing [38,39]. Only ponderomotive self-focusing was considered when deriving the FFOM. Grech *et al.* suggested the addition of two terms: $\gamma_T = 1 + 1.76Z^{5/7}(\rho_0/\lambda_{ei})^{4/7}$, where ρ_0 is the transverse speckle width and λ_{ei} the electron-ion mean free path, to account for thermally enhanced excitation of ion waves; and the inverse normalized ion acoustic wave damping rate $(\omega/\nu)_{IAW}$ to allow for

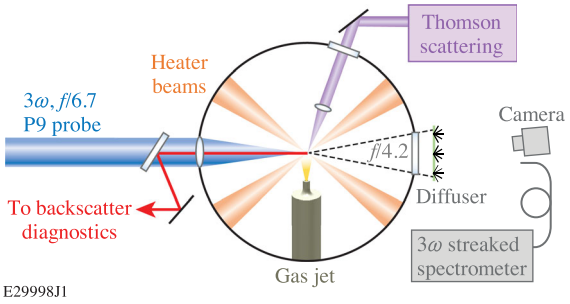

FIG. 1. Experimental setup.

the possibility of weak damping [31,40]. These additions were intended to better capture the role of ion acoustic waves in the FSBS-dominated moderate-intensity regime, giving

$$\gamma_T \left(\frac{\omega}{\nu}\right)_{\mathrm{IAW}} \langle I_{14}\rangle \lambda^2 \frac{n_e}{n_c}\frac{3}{T_e}\left(\frac{f^{\#}}{8}\right)^2 > 1. \quad (1)$$

This generalized (or Grech) figure of merit (GFOM) remained largely untested.

Previous experiments achieved important milestones including observations of filaments [23,41], beam spray [32,39,42–44], frequency shifts [32,42,43], induced incoherence [33,34,45], and improved beam propagation with the use of smoothing techniques [23,38,43,44,46]. However, this early work was typically affected by some or all of the following: limited plasma characterization, poor data quality, extreme drive conditions, low beam transmission, scant data, and little quantification of angular spreading and redshifting—arguably the most important observables.

In this Letter, we present experimental results demonstrating the need to account for thermal enhancement of ion acoustic waves, as well as a dependence on ion acoustic wave damping, to determine the level of beam spray caused by FSBS. The results were obtained in a platform designed to isolate beam spray from other competing instabilities, with high transmission and well-characterized plasma conditions enabling careful accounting of laser energetics. The inferred thresholds range from ≈2 to 15× lower than the previous theory, which can drastically affect expectations for beam spray. The wavelength shifts in the transmitted beam are comparable to those generating significant symmetry swings in recent LID implosions. They also grow continuously for several hundred ps despite the drive remaining relatively constant, which may pose a key challenge to developing a reduced model of beam spray for incorporation into radiation-hydrodynamic codes [47].

The experiments were performed at the University of Rochester's Laboratory for Laser Energetics using the recently commissioned LPI platform shown in Fig. 1 [48–50]. A supersonic gas jet with a 2-mm-exit-diam nozzle provided a uniform volume of gas at target chamber center [51]. The gas was ionized and heated quasi-isotropically by 11 OMEGA beams, each with nearly 200 J in a 500-ps square pulse shape and conditioned with "SG5" phase plates to have a 714-μm-FWHM far-field diameter. For this campaign, temporally resolved electron-feature Thomson scattering was fielded to measure density and temperature (based on a super-Gaussian assumption for the electron distribution function [48,49]) in the center of the plasma (values are reported in Table I). In addition, spatially resolved Thomson scattering from a different campaign featuring the same nozzles and standoff distance along with a similar heating configuration indicate that the plasma spatial profile was close to Gaussian both in terms of density (1.47-mm FWHM) and temperature (1.37-mm FWHM).

The P9 probe beam—in this case 3ω although there are options for 2ω, tunable 3ω [52], or 4ω—was injected at $t = 0.6$ ns (immediately after the heater beams turned off). It was linearly polarized and conditioned using an "LLNL-3ω-150" phase plate to have a 118-μm-FWHM diameter at best focus, enabling average intensities up to 1.7×10^{15} W/cm^2. Like the heater beams, it was on for 500 ps.

After propagating through the plasma, the probe beam was diagnosed using the transmitted beam diagnostic [53]. The beam terminated outside the vacuum chamber on a spectralon diffuser plate located 1.9 m from the target chamber center and with an $f/4.2$ clear aperture, which enabled full accounting of the beam even in cases with significant beam spray. The rescattered light off the diffuser

TABLE I. Shot summary.

Ω#101-	Gas	$\langle I_{14}\rangle$	n_e (10^{20} cm^{-3})	T_e (keV)	γ_T	$(v/\omega)_{\mathrm{IAW}}$	Transmission (%)	SBS (%)	SRS (%)	Absorption (%)	Total (%)
−402	N_2	7.4	3.91	1.13	3.2	0.02	55.4	21.7	0.0	15.1	92.2
−403	N_2	15.3	3.98	1.23	3.0	0.02	40.1	37.2	0.0	12.9	90.2
−404	N_2	3.6	3.96	1.13	3.2	0.02	66.6	4.3	0.0	16.9	87.9
−406	CH_4	7.2	4.04	0.95	2.3	0.1–0.5	65.1	1.0	2.8	12.9	81.9
−407	CH_4	15	3.86	1.01	2.2	0.1–0.5	56.0	5.3	4.5	10.0	75.8
−408	CH_4	3.5	4.15	0.92	2.4	0.1–0.5	74.6	0.7	0.1	15.2	90.7
−413	CH_4	7.1	2.05	0.79	2.1	0.1–0.5	95.7	< 0.2	0.0	4.2	100.2
−414	CH_4	15.8	2.02	0.89	1.9	0.1–0.5	93.1	3.1	0.8	3.2	100.2
−415	CH_4	3.5	2.26	0.75	2.2	0.1–0.5	93.6	< 0.2	0.0	5.9	99.7

plate was sampled in transmission by a time-integrated camera as well as a fiber-coupled uv streaked spectrometer that measured the power and spectrum with ≈60-ps and 0.4-Å temporal and spectral resolution, respectively.

For a more complete picture of the processes impacting the beam propagation, direct backscatter was also monitored. A Fresnel reflection off of a full-aperture uncoated wedged pickoff directed a portion of the light recollimated by the focus lens to a pair of absolutely calibrated cameras, one filtered for stimulated Brillouin scattering (SBS) and one filtered for stimulated Raman scattering (SRS).

The campaign featured a three-shot intensity scan in CH_4 at $n_e \approx 4 \times 10^{20}$ cm^{-3}, another in N_2 at the same electron density, and a third in CH_4 at half the electron density. Varying the ion composition and density resulted in diversity of both the ion acoustic wave damping and the thermal enhancement factor γ_T [Eq. (1)]. A shot summary is shown in Table I, including the probe intensity (±5% uncertainty), electron density (±2%), and temperature (±5%) in the center of the plasma, time-averaged over the probe duration; measured transmission (±2%); SBS reflectivity (±10%); SRS reflectivity (±20%); calculated absorption (±4%); and the total that sums transmission, backscatter, and expected absorption. The high transmission and low backscatter in low-density CH_4 allowed near-perfect accounting of the laser propagation, providing ideal conditions for studying the onset of beam spray in isolation. At higher density, backscatter began to affect the beam propagation. The shots with the most "missing energy" were those with significant SRS—consistent with other recent findings [8]—a deficit that is likely caused in part by Raman sidescatter [54]. In N_2, the gap is likely due in large part to backscatter spraying outside the collection lens (no attempt at extrapolation was made).

Beam spray was assessed using the time-integrated images recorded by the transmitted beam diagnostic. Four methane shots spanning the full range of data are shown in Fig. 2(a). The angular spreading was quantified by finding the average radial lineout, normalizing it by the signal level near the center of the beam, and then identifying the radius where the signal is nearest 10% of the normalized value (denoted R_{10}). The lineouts for these shots are shown in Fig. 2(b), and the contours are also marked with dashed black curves in Fig. 2(a). (Note that shot 101 407—which had the most beam spray—is impacted by clipping the edge of the diffuser plate, so the transmission reported in Table I is underestimated. Only the half of the plate that better captured the edge of the beam was used for the radial lineout in that case.)

The first key result is shown in Fig. 2(c), which plots the 10% intensity contour normalized by that of the beam propagating through vacuum (13.8 cm). The uncertainty is approximately the marker size. Following the convention of Ref. [31], they are plotted versus the ratio of the average power per speckle to the critical power for self-focusing

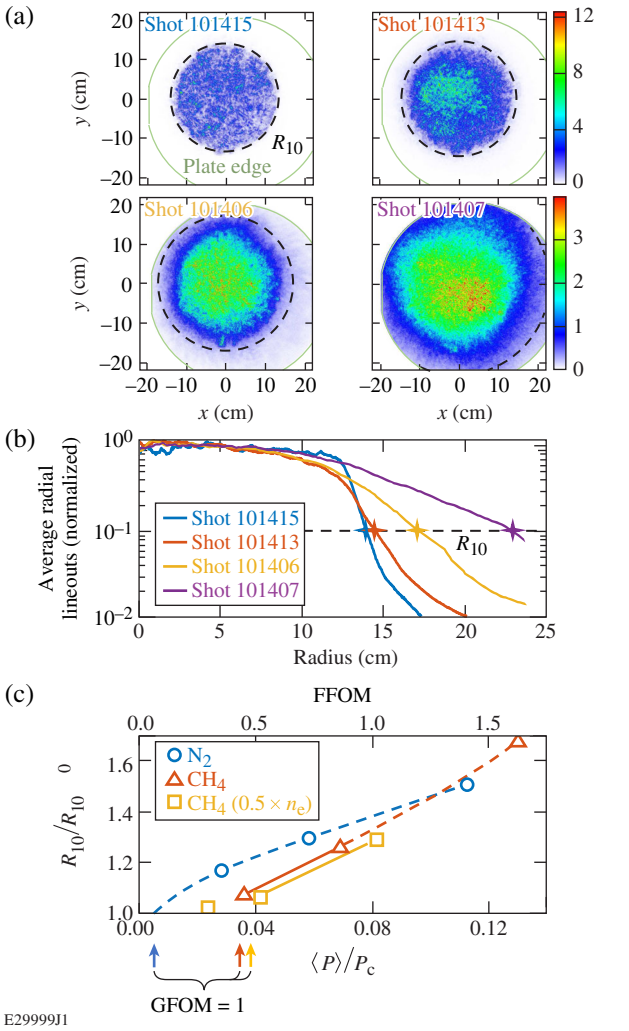

FIG. 2. Beam spray results. (a) Raw data for four of the shots are shown along with the 10% intensity contours based on the average radial lineouts shown in (b). (c) Normalized values of these 10% contours are plotted versus the ratio of the average power per speckle to the critical power for self-focusing (lower axis) as well as the filamentation figure of merit (upper axis). Beam spray occurs below FFOM = 1 in all cases but has a particularly low threshold in nitrogen due to weak ion acoustic wave damping.

$\langle P \rangle / P_c$, where $\langle P \rangle = \pi \rho_0^2 \langle I \rangle$, $\rho_0 = (2/\pi) f^{\#} \lambda = 1.5$ μm is the speckle radius, and $P_c = (8\pi/k_0^2) c T_e n_c^2 / n_e \approx$ 0.7–1.3 GW depending on the shot. Note that the calculated far-field spatial profile of the beam based on measurements of the phase plate that was used gives characteristic feature sizes in good agreement with the speckle radius indicated above. The fact that $\langle P \rangle / P_c \ll 1$ underscores the fact that few if any speckles have enough power to self-focus, putting these results squarely in the pure-FSBS regime. The FFOM—related to $\langle P \rangle / P_c$ by a scalar factor (≈12.5)—is also shown along the top for reference. This makes it clear that the onset of beam spray is occurring below FFOM = 1 in each case. The use of $\langle P \rangle / P_c$ also

allows the expected threshold (Eq. (1): GFOM = 1) to be written as $\langle P\rangle/P_c = \sqrt{2/\pi}(\nu/\omega)(1/\gamma_T)$, which is indicated by the arrow for each dataset. It is clear that the GFOM reliably predicts the onset of beam spray in each case.

The N_2 results stand out from the CH_4 shots. The dashed curve is provided simply to guide the eye, but it shows that the points could be consistent with the expected threshold, which is low ($\langle P\rangle/P_c = 0.005$) both because of weak ion Landau damping ($\nu/\omega \approx 0.02$) and a large thermal enhancement factor ($\gamma_T \approx 3.1$). The fact that the curve is concave down and eventually intersects the CH_4 data is suggestive of saturation likely caused by pump depletion. Weak damping promotes competition with backward SBS, and only the light that transmits through the backscatter region will drive beam spray [24,26]. The relatively low values of transmission and associated high SBS reflectivities listed in Table I are consistent with this picture.

Beam spray in CH clearly turns on at a higher intensity, which is primarily due to the large difference in ion Landau damping: $\nu/\omega \approx 0.1$ to 0.5 for $T_i/T_e = 0.1$ to 0.2. (The fact that ion temperature was not measured in these experiments is a source of uncertainty, but we typically find ion-to-electron temperature ratios in this range for gas jet experiments [48,55].) The low-density, low-intensity shot (101 415) had almost no change in the measured beam diameter relative to the vacuum case. Linear fits though two points of each dataset are shown to highlight the slight offset between the two different densities. The roughly 10% difference is actually consistent with the expectations from Eq. (1) due to slightly different thermal enhancement factors (2.3 versus 2.1). Note the arrows indicating GFOM = 1 assume $\nu/\omega = 0.1$.

The second key result pertains to the wavelength shifts shown in Fig. 3. Figure 3(a) shows a sample time-resolved transmitted beam spectrum from shot 101 402, which has two main contributions: the FSBS shift from the actual beam spray, and the so-called "Dewandre" shift resulting from plasma density along the probe path changing in time due to hydrodynamic expansion [56]. To isolate the former, the latter must be removed. The Dewandre shift was estimated two ways. First, the expected shift was modeled using the time-resolved density information in the center of the plasma along with two assumptions: (1) the plasma profile is Gaussian and spherically symmetric per the complementary imaging Thomson scattering information mentioned earlier, and (2) the plasma conserves electrons as it expands. The result of this calculation for shot 101 402 is shown in Fig. 3(a). Second, the frequency shift from beam spray is intensity-dependent whereas the Dewandre shift is not. Therefore, the measured shift at very early and late time should be entirely due to the changing plasma density, so a linear fit through points at $t = 0.65$ and $t = 1.35$ ns provided the second estimate. The two estimates agreed well, particularly for the nitrogen shots.

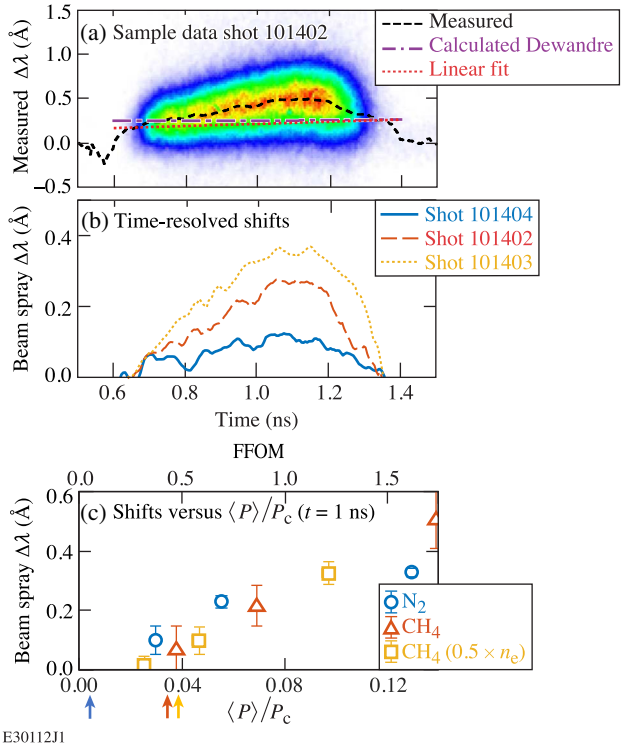

FIG. 3. Frequency shifts. (a) An example (shot 101 402) of the transmitted beam time-resolved spectrum is shown. The dashed black curve shows the time-dependent centroid of the spectrum. There are two main contributions to the measured frequency shift: beam spray and the so-called Dewandre shift. (b) The beam spray frequency shifts evidently continue increasing for several hundred ps despite steady drive conditions, indicating the time to reach steady state is quite long. (c) A plot of the frequency shifts at $t = 1 \pm 0.05$ ns versus FFOM bears a very similar resemblance to the plot of R_{10} versus FFOM in Fig. 2(c), suggesting a direct correspondence between the magnitude of the frequency shift and the amount of spray, as expected.

Given uncertainty regarding the actual plasma spatial profiles, the linear fits were assumed to be more reliable and were used in the subsequent analysis.

Although the laser power, $\langle P\rangle/P_c$, and the FFOM were relatively constant (typically to better than 10%) for ≈300 to 400 ps during the middle of the pulse, Fig. 3(b) shows that the beam spray wavelength shifts continue increasing with time, resulting in significant negative skewness to the time history. Simulations have also observed FSBS growth times from hundreds of ps to several ns [28,31]. Typically, we expect SBS saturation times $\approx 1/\nu$. Since the damping rate decreases with scattering angle, the time dependence suggests scattering angles $< 1°$, particularly for the more strongly damped CH plasmas. In turn, this implies that the observed beam spray results from multiple small-angle FSBS events (the transmitted beam half-angle increased from 4.2° to as much as 7°). Multiple FSBS have also been seen in simulations [27,28]. Since reduced LPI models that

have been incorporated into radiation-hydrodynamics codes are typically steady-state models that assume saturation times much shorter than hydrodynamic timescales, the long timescales we observe here pose a key challenge for the development of such a reduced model describing beam spray [47].

The dependence of the beam spray wavelength shift on $\langle P \rangle / P_c$ is shown in Fig. 3(c). The plot resembles Fig. 2(c) quite closely, suggesting a direct correspondence between the amount of beam spray and the magnitude of the wavelength shift, as expected. The trend in the nitrogen data is once again indicative of a lower threshold (due to weak ion acoustic wave damping) and nonlinear saturation due to pump depletion at the highest intensity.

In summary, the thresholds for beam spray can be a factor of 2 to 15× less than the oft-cited FFOM would suggest, but they are well predicted by the GFOM. Recalling the specific question that motivated this Letter regarding what impacts, if any, might result from the outer cones nearing FFOM = 1 in the Al plasma outside the entrance of a National Ignition Facility hohlraum, the nitrogen results are most pertinent because $(\nu/\omega)_{\mathrm{IAW}} \propto T_i/(ZT_e)$ so weak damping is applicable. Thus, significant beam spray may be expected. Furthermore, the maximum wavelength shifts presented here exceeded 0.5 Å at 3ω. Using the National Ignition Facility convention, that is equivalent to 1.5 Å at 1ω, and implosion symmetry has recently been shown to be highly sensitive to wavelength detuning in modern hohlraums (≈20 to 50 μm-P2/Å at 1ω [11–15]). Therefore, cone-specific beam spray occurring outside the hohlraum is highly likely to compromise symmetry control, and avoiding this situation should be a high priority for target design.

This material is based upon work supported by the DOE NNSA under Award No. DE-NA0003856, DOE/FES under Award No. DE-SC00221032, the University of Rochester, and the New York State Energy Research and Development Authority. This Letter was prepared as an account of work sponsored by an agency of the U.S. Government. Neither the U.S. Government nor any agency thereof, nor any of their employees, makes any warranty, express or implied, or assumes any legal liability or responsibility for the accuracy, completeness, or usefulness of any information, apparatus, product, or process disclosed, or represents that its use would not infringe privately owned rights. Reference herein to any specific commercial product, process, or service by trade name, trademark, manufacturer, or otherwise does not necessarily constitute or imply its endorsement, recommendation, or favoring by the U.S. Government or any agency thereof. The views and opinions of authors expressed herein do not necessarily state or reflect those of the U.S. Government or any agency thereof.

*Corresponding author.
turnbull@lle.rochester.edu

[1] D. H. Froula, D. T. Michel, I. V. Igumenshchev, S. X. Hu, B. Yaakobi, J. F. Myatt, D. H. Edgell, R. Follett, V. Y. Glebov, V. N. Goncharov, T. J. Kessler, A. V. Maximov, P. B. Radha, T. C. Sangster, W. Seka, R. W. Short, A. A. Solodov, C. Sorce, and C. Stoeckl, Plasma Phys. Controlled Fusion **54**, 124016 (2012).
[2] E. Campbell *et al.*, Matter Radiat. Extremes **2**, 37 (2017).
[3] S. Laffite and P. Loiseau, Phys. Plasmas **17**, 102704 (2010).
[4] R. K. Kirkwood, J. D. Moody, J. Kline, E. Dewald, S. Glenzer, L. Divol, P. Michel, D. Hinkel, R. Berger, E. Williams, J. Milovich, L. Yin, H. Rose, B. MacGowan, O. Landen, M. Rosen, and J. Lindl, Plasma Phys. Controlled Fusion **55**, 103001 (2013).
[5] T. Gong *et al.*, Matter Radiat. Extremes **4**, 055202 (2019).
[6] M. Geissel *et al.*, Phys. Plasmas **25**, 022706 (2018).
[7] L. F. Berzak Hopkins *et al.*, Phys. Rev. Lett. **114**, 175001 (2015).
[8] G. N. Hall, O. S. Jones, D. J. Strozzi, J. D. Moody, D. Turnbull, J. Ralph, P. A. Michel, M. Hohenberger, A. S. Moore, O. L. Landen, L. Divol, D. K. Bradley, D. E. Hinkel, A. J. Mackinnon, R. P. J. Town, N. B. Meezan, L. Berzak Hopkins, and N. Izumi, Phys. Plasmas **24**, 052706 (2017).
[9] S. LePape *et al.*, Phys. Rev. Lett. **120**, 245003 (2018).
[10] K. L. Baker *et al.*, Phys. Rev. Lett. **121**, 135001 (2018).
[11] A. L. Kritcher, J. Ralph, D. E. Hinkel, T. Döppner, M. Millot, D. Mariscal, R. Benedetti, D. J. Strozzi, T. Chapman, C. Goyon, B. MacGowan, P. Michel, D. A. Callahan, and O. A. Hurricane, Phys. Rev. E **98**, 053206 (2018).
[12] L. A. Pickworth *et al.*, Phys. Plasmas **27**, 102702 (2020).
[13] A. L. Kritcher *et al.*, Phys. Plasmas **28**, 072706 (2021).
[14] A. B. Zylstra *et al.*, Phys. Rev. Lett. **126**, 025001 (2021).
[15] J. S. Ross *et al.*, arXiv:2111.04640.
[16] T. Doeppner, S. A. MacLaren, O. L. Landen, D. E. Hinkel, P. A. Amendt, J. E. Ralph, A. B. Zylstra, A. L. Kritcher, and J. C. Delora-Ellefson, Impact of external LEH hardware on implosion shape and laser-to-hohlraum coupling in indirect drive implosions at the National Ignition Facility, in *Proceedings of the 63rd Annual Meeting of the APS Division of Plasma Physics, 2021* (unpublished), https://meetings.aps.org/Meeting/DPP21/Session/GO04.8.
[17] P. Kaw, G. Schmidt, and T. Wilcox, Phys. Fluids **16**, 1522 (1973).
[18] F. W. Perkins and E. J. Valeo, Phys. Rev. Lett. **32**, 1234 (1974).
[19] E. M. Epperlein, Phys. Rev. Lett. **65**, 2145 (1990).
[20] C. E. Max, J. Arons, and A. B. Langdon, Phys. Rev. Lett. **33**, 209 (1974).
[21] A. J. Schmitt, Phys. Fluids **31**, 3079 (1988).
[22] A. J. Schmitt, Phys. Fluids B **3**, 186 (1991).
[23] C. Labaune, S. Baton, T. Jalinaud, H. A. Baldis, and D. Pesme, Phys. Fluids B **4**, 2224 (1992).
[24] V. V. Eliseev, W. Rozmus, V. T. Tikhonchuk, and C. E. Capjack, Phys. Plasmas **2**, 1712 (1995).
[25] P. Michel, C. Labaune, S. Weber, V. T. Tikhonchuk, G. Bonnaud, G. Riazuelo, and F. Walraet, Phys. Plasmas **10**, 3545 (2003).

[26] V. V. Elisseev, I. Ourdev, W. Rozmus, V. T. Tikhonchuk, C. E. Capjack, and P. E. Young, Phys. Plasmas **4**, 4333 (1997).
[27] A. J. Schmitt and B. B. Afeyan, Phys. Plasmas **5**, 503 (1998).
[28] A. V. Maximov, I. G. Ourdev, D. Pesme, W. Rozmus, V. T. Tikhonchuk, and C. E. Capjack, Phys. Plasmas **8**, 1319 (2001).
[29] M. Grech, V. T. Tikhonchuk, G. Riazuelo, and S. Weber, Phys. Plasmas **13**, 093104 (2006).
[30] P. M. Lushnikov and H. A. Rose, Plasma Phys. Controlled Fusion **48**, 1501 (2006).
[31] M. Grech, G. Riazuelo, D. Pesme, S. Weber, and V. T. Tikhonchuk, Phys. Rev. Lett. **102**, 155001 (2009).
[32] J. Fuchs, C. Labaune, S. Depierreux, H. A. Baldis, A. Michard, and G. James, Phys. Rev. Lett. **86**, 432 (2001).
[33] V. Malka, J. Faure, S. Hüller, V. T. Tikhonchuk, S. Weber, and F. Amiranoff, Phys. Rev. Lett. **90**, 075002 (2003).
[34] S. Depierreux *et al.*, Phys. Rev. Lett. **102**, 195005 (2009).
[35] H. A. Rose, Phys. Plasmas **3**, 1709 (1996).
[36] D. E. Hinkel, E. A. Williams, and C. H. Still, Phys. Rev. Lett. **77**, 1298 (1996).
[37] J. D. Moody, B. J. MacGowan, D. E. Hinkel, W. L. Kruer, E. A. Williams, K. Estabrook, R. L. Berger, R. K. Kirkwood, D. S. Montgomery, and T. D. Shepard, Phys. Rev. Lett. **77**, 1294 (1996).
[38] E. L. Dewald, S. H. Glenzer, O. L. Landen, L. J. Suter, O. S. Jones, J. Schein, D. Froula, L. Divol, K. Campbell, M. S. Schneider, J. Holder, J. W. McDonald, C. Niemann, A. J. Mackinnon, and B. A. Hammel, Plasma Phys. Controlled Fusion **47**, B405 (2005).
[39] D. H. Froula, L. Divol, N. B. Meezan, S. Dixit, J. D. Moody, P. Neumayer, B. B. Pollock, J. S. Ross, and S. H. Glenzer, Phys. Rev. Lett. **98**, 085001 (2007).
[40] A. V. Brantov, V. Y. Bychenkov, V. T. Tikhonchuk, W. Rozmus, and V. K. Senecha, Phys. Plasmas **6**, 3002 (1999).
[41] P. E. Young, H. A. Baldis, R. P. Drake, E. M. Campbell, and K. G. Estabrook, Phys. Rev. Lett. **61**, 2336 (1988).
[42] S. H. Batha, K. S. Bradley, H. A. Baldis, R. P. Drake, K. Estabrook, T. W. Johnston, and D. S. Montgomery, Phys. Rev. Lett. **70**, 802 (1993).
[43] J. D. Moody, B. J. MacGowan, S. H. Glenzer, R. K. Kirkwood, W. L. Kruer, A. J. Schmitt, E. A. Williams, and G. F. Stone, Phys. Rev. Lett. **83**, 1783 (1999).
[44] C. Niemann, L. Divol, D. H. Froula, G. Gregori, O. Jones, R. K. Kirkwood, A. J. MacKinnon, N. B. Meezan, J. D. Moody, C. Sorce, L. J. Suter, R. Bahr, W. Seka, and S. H. Glenzer, Phys. Rev. Lett. **94**, 085005 (2005).
[45] J. Fuchs, C. Labaune, H. Bandulet, P. Michel, S. Depierreux, and H. A. Baldis, Phys. Rev. Lett. **88**, 195003 (2002).
[46] S. H. Glenzer *et al.*, Nat. Phys. **3**, 716 (2007).
[47] C. Ruyer, A. Debayle, P. Loiseau, P. E. Masson-Laborde, J. Fuchs, M. Casanova, J. R. Marquès, L. Romagnani, P. Antici, N. Bourgeois, M. Nakatsutsumi, M. Safronova, M. Starodubtsev, and T. Lin, Phys. Plasmas **28**, 052701 (2021).
[48] D. Turnbull, A. Colaitis, A. M. Hansen, A. L. Milder, J. P. Palastro, J. Katz, C. Dorrer, B. E. Kruschwitz, D. J. Strozzi, and D. H. Froula, Nat. Phys. **16**, 181+ (2020).
[49] A. L. Milder, J. Katz, R. Boni, J. P. Palastro, M. Sherlock, W. Rozmus, and D. H. Froula, Phys. Rev. Lett. **127**, 015001 (2021).
[50] A. M. Hansen, K. L. Nguyen, D. Turnbull, B. J. Albright, R. K. Follett, R. Huff, J. Katz, D. Mastrosimone, A. L. Milder, L. Yin, J. P. Palastro, and D. H. Froula, Phys. Rev. Lett. **126**, 075002 (2021).
[51] A. M. Hansen, D. Haberberger, J. Katz, D. Mastrosimone, R. K. Follett, and D. H. Froula, Rev. Sci. Instrum. **89**, 10C103 (2018).
[52] B. E. Kruschwitz, J. Kwiatkowski, C. Dorrer, M. Barczys, A. Consentino, D. H. Froula, M. J. Guardalben, E. M. Hill, D. Nelson, M. J. S. III, D. Turnbull, L. J. Waxer, and D. Weiner, in *High Power Lasers for Fusion Research V*, edited by A. A. S. Awwal and C. L. Haefner, International Society for Optics and Photonics (SPIE, 2019), Vol. 10898, pp. 22–33.
[53] J. Katz, D. Turnbull, B. E. Kruschwitz, A. L. Rigatti, R. Rinefierd, and D. H. Froula, Rev. Sci. Instrum. **92**, 033526 (2021).
[54] Y.-J. Gu, O. Klimo, V. Tikhonchuk, and S. Weber, Nucl. Fusion **61**, 066014 (2021).
[55] D. Turnbull, C. Goyon, G. E. Kemp, B. B. Pollock, D. Mariscal, L. Divol, J. S. Ross, S. Patankar, J. D. Moody, and P. Michel, Phys. Rev. Lett. **118**, 015001 (2017).
[56] T. Dewandre, J. R. Albritton, and E. A. Williams, Phys. Fluids **24**, 528 (1981).